Aerosol Science and Engineering
https://doi.org/10.1007/s41810-021-00103-8

ORIGINAL PAPER

Investigation of Chemical Composition and Fiber-Occurrence in Inhalable Particulate Matter Obtained from Dry Cutting Processes of Carbon Fiber Reinforced Concrete Composite, Concrete and the Carbon Fiber Reinforcement Materials

Arne Koch[1] · **Paul Bergelt**[2] · **Petra Fiala**[2] · **Uwe Käfer**[1] · **Jürgen Orasche**[3] · **Stefanie Bauer**[3] · **Sebastiano Di Bucchianico**[3] · **Michael Stintz**[2] · **Thomas Gröger**[3] · **Thorsten Streibel**[1,3] · **Ralf Zimmermann**[1,3]

Received: 11 January 2021 / Revised: 30 April 2021 / Accepted: 6 May 2021

Abstract

The most commonly used construction material nowadays is steel-reinforced concrete which underlies corrosion and thus buildings are susceptible for structural collapses. Recently, a new construction material resistant to oxidation and with a higher tensile strength called carbon concrete composite (C^3) was developed. The new material allows resource-saving constructions using carbon fiber instead of steel reinforcement materials embedded in a concrete matrix. C^3 reinforcements consist of carbon fibers coated with an organic polymer matrix. In this study, abrasive dust from a dry cutting process of two C^3 reinforcement materials, as well as a C^3 material were investigated with respect to the occurrence of toxic fibers or harmful organic compounds in the inhalable particulate matter (PM) fractions $PM_{2.5}$ and PM_{10}. It could be shown that the ratio between elemental and organic carbon in PM_{10} is dependent on the shape of the C^3 reinforcement material due to different mechanisms of PM formation. This could have an impact on the toxicity of different C^3 reinforcement materials. Harmful fibers according to the World Health Organization (WHO) definition like they are found in asbestos concrete were not found. However, bisphenol A (BPA) as well as the PAHs phenanthrene, anthracene, fluoranthene and pyrene were found due to pyrolysis of the organic matrix material at the edge of the sawblade differentiating the Carcinogenic Equivalency (TEQ) of investigated materials and their PM fractions. Furthermore, derivatives of BPA occurred in abrasive dust from C^3 reinforcement materials potentially leading to genotoxicity and reproductive toxicity.

Keywords Construction material · Carbon fiber reinforced concrete composite · Dry cutting process · Inhalable particulate matter · Bisphenol A · Polycyclic aromatic hydrocarbons

Abbreviations

BaP	Benzo(a)pyrene
BPA	Bisphenol A
BW	Body weight
IR	Inhalation rate
C^3	Carbon concrete composite
EC	Elemental carbon
ER	Exposure rate
FID	Flame ionization detector
OC	Organic carbon
PAH	Polycyclic aromatic hydrocarbon
PM	Particulate matter
PAN	Polyacrylonitrile
PIMS	Photoionization mass spectrometry
REMPI	Resonance-enhanced multi photon ionization
SEM	Scanning electron microscopy
S/N	Signal-to-noise
SBR	Styrene-butadiene rubber
SPI	Single photon ionization
TEF	Toxic equivalent factor
TEQ	Toxic equivalent

✉ Thorsten Streibel
thorsten.streibel@uni-rostock.de

[1] Department of Analytical Chemistry, University of Rostock, Dr.-Lorenz-Weg 2, 18059 Rostock, Germany

[2] Department of Mechanical Process Engineering, Technical University of Dresden, Münchner Platz 3, 01187 Dresden, Germany

[3] Joint Mass Spectrometry Center, Comprehensive Molecular Analytics, Helmholtz-Zentrum München, Ingolstädter Landstraße 1, 85764 Neuherberg, Germany

TOCA	Thermo-optical carbon analyzer
WHO	World Health Organization

1 Introduction

Concrete is the most important construction material nowadays as well as for the foreseeable future. Due to its brittleness, a lot of effort was put into research to its strengthening and to achieve a better ductility. The most commonly found concrete-based building material today is steel-reinforced concrete using steel rods as reinforcement material. However, steel corrodes under various conditions such as marine or air environment leading to cracks in steel-reinforced concrete. Fiber-reinforced concretes could serve as an alternative exhibiting a higher longevity. Thus, e.g. randomly distributed short asbestos (Mai 1979; Lenain and Bunsell 1979), glass (Ghugal and Deshmukh 2006; Kizilkanat et al. 2015), basalt (Kizilkanat et al. 2015; Fiore et al. 2015) or carbon (Chung 2000; Wang et al. 2008) fibers were used as reinforcement materials. While asbestos fibers were found to cause health impairments such as asbestosis or lung cancer due to their morphology (Felley-Bosco and MacFarlane 2018), glass and basalt fibers showed a poor resistance against alkaline environments, such as in a cementitious matrix (Sim et al. 2005; Lee et al. 2014). A higher longevity is expected when carbon fibers are used as reinforcement material due to their resistance to alkaline and corrosive environments (Sim et al. 2005; Spelter et al. 2019; Böhm et al. 2018). Furthermore, continuous, unidirectional fibers are expected to have a higher positive impact on the ductility and tensile strength than short randomly distributed fibers (Chung 2000).

Therefore, carbon concrete composites (C^3) with a five-fold tensile strength compared to steel-reinforced concrete were developed a few years ago (Bienkowski et al. 2018). They allow resource-saving constructions using grids or rods out of carbon fibers as a reinforcement material for concrete. The carbon fibers for these materials are most often based on a polyacrylonitrile (PAN) or pitch precursor, which is stabilized at 200–400 °C (Böhm et al. 2018; Frank et al. 2014; Jäger et al. 2016; Morgan 2005) under air conditions and afterwards carbonized at 400–1600 °C (Böhm et al. 2018; Frank et al. 2014; Jäger et al. 2016; Morgan 2005) under nitrogen conditions. Higher tensile strength can be achieved via graphitization at temperatures up to 3000 °C (Frank et al. 2014; Jäger et al. 2016; Morgan 2005) in a third step. As a result, oxygenation, dehydrogenation and cyclization of the PAN fiber occurs and a carbon fiber with > 98% (Frank et al. 2014) carbon fraction is formed (Böhm et al. 2018; Frank et al. 2014; Jäger et al. 2016; Morgan 2005). Due to the production process, the fibers have diameters of ~ 7 µm (Hillemann et al. 2018). To obtain the reinforcement material, up to 48,000 carbon fibers are combined and bound in a polymer matrix, such as styrene-butadiene rubber (SBR), polyacrylate or epoxy resin to form a so-called roving. Furthermore, the polymer matrix improves the grip between the carbon fibers and the concrete and thus increases the stability of the C^3. Carbon grids are obtained by weaving of rovings (Morgan 2005; Hillemann et al. 2018). During their lifecycle as construction material, C^3 materials will be exposed to stress situations such as abrasive processing, which could lead to the production of harmful organic compounds or fibers similar to asbestos fibers according to the World Health Organization (WHO) definition [TRGS905 (BAuA 2020), (> 5 µm length, < 3 µm diameter, length/diameter > 3)].

Only a few studies addressed the release of chemical substances or the potential formation of harmful fibers during the handling of C^3 and the involved potential health issues. Most research focuses on physical performance parameters, such as tensile strength and torsional strength. Studies on chemical parameters and fiber morphology are rare. Weiler and Vollpracht (2019) studied the leaching of C^3 and the release of heavy metals and trace elements during rain scenarios, but found no environmentally harmful concentrations. Bienkowski et al. (2018) and Hillemann et al. (2018) showed that no harmful fibers according to the WHO definition were observed in crushing or cutting processes of C^3. However, they found carbon fibers with diameters of ~ 7 µm in the total dust fraction. Furthermore, Hillemann et al. (2018) showed that organic trace compounds from the organic matrix of the carbon fibers can be found in the gas phase produced by dry cutting processes. In contrast, the particle phase of the aerosol from dry cutting processes was not sufficiently investigated yet. After inhalation, particulate matter (PM) with an aerodynamic diameter ≤ 10 µm (PM_{10}) and ≤ 2.5 µm ($PM_{2.5}$) can enter the respiratory system and be deposited in the tracheobronchial tree and the alveoli, respectively. Deposited PM deep in the gas exchange system might impair the lung function and lead to health impairments (Kim et al. 2015; Harrison and Yin 2000). Thus, the aim of this work was to investigate the inhalable PM fractions PM_{10} and $PM_{2.5}$ produced from dry cutting processes of C^3 and their reinforcement materials with respect to the occurrence of harmful fibers and organic compounds.

2 Materials and Methods

2.1 Samples and Equipment

Two commercially available C^3 reinforcement materials from different manufacturers were investigated, one rod-shaped (carbon rod) and one grid-shaped (carbon grid). According to the manufacturers, both materials contain fibers based on PAN and are coated with an epoxy resin. Furthermore, a concrete containing one layer of the grid-shaped reinforcement material as well as the pure concrete as a reference sample were studied. For the production of the concrete plates, a pouring process was used. The concrete was poured into a 33 cm × 38 cm × 1.8 cm rectangular form. Additionally, the reinforcement material was set into the middle of the concrete and the concrete was stored in a dry environment. An “Abrasive Dust Generator” from Vitrocell (Waldkirch, GER) equipped with a diamond sawblade was used to produce PM from the samples by a dry cutting process. Additionally, an aerosol particle sizer “LAP 322” from Topas (Dresden, GER) and a filter control device “LVS3.1” from Comde-Derenda (Stahnsdorf, GER) were used for aerosol sampling. Quartz fiber (47 mm, grade T293) and methylcellulose filters (47 mm, 1.2 µm) were purchased from Munktell and GE Healthcare Life Sciences, respectively. Quartz fiber filters were heated to 550 °C for 12 h prior to sample preparation. Furthermore, bisphenol A (BPA) as a reference substance was purchased at TCI (Eschborn, GER) with a purity of > 99%. Gases used for analysis had a purity of > 99.9% and were used without further purification.

2.2 Sample Preparation

For the preparation of filter samples, the concrete plates and reinforcement materials were cut by the Abrasive Dust Generator in a dry cutting simulation with a rotation of the sawblade of 50 Hz and a cutting speed of 0.1 mm/s and 0.2 mm/s, respectively. The cutting was performed along the rovings to produce the highest amounts of possibly harmful chemical substances and fibers. Concrete plates and carbon rods were cut with a cutting depth of 10 mm and 3 mm, respectively. It was always ensured that the carbon grid contained in the concrete was cut through in its full depth. Five layers of carbon grid were aligned and fixed to each other to cut the carbon grid properly. The resulting arrangement was cut with a cutting depth of 5 mm. As a result, two and a half layers of carbon grid were cut through. Figure 1 shows a C^3 plate and the reinforcement materials (a–c) as well as a schematic illustration of the dry cutting sample preparation arrangement (d). The dust produced from the abrasive dust generator was extracted at the sawblade edge with a flow of 71 m^3/h. The dust was split via an isokinetic sampling into a fraction of 98.58% that was discarded and a fraction of 1.42% that was used for the analyses. In a second isokinetic sampling 0.01% of the dust was transferred to the aerosol particle sizer to measure the particle size distribution. The remaining fraction of 1.41% with a flow of 1.0

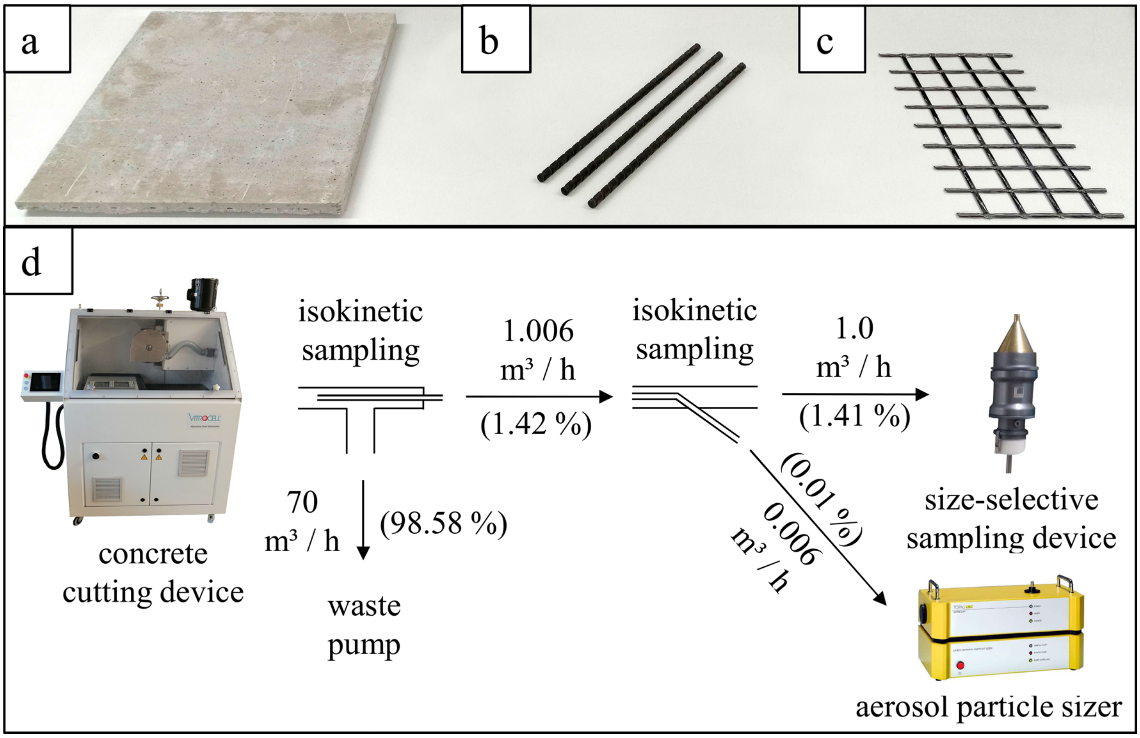

Fig. 1 Pictures of the C^3 material (**a**), carbon rods (**b**), carbon grid (**c**) as well as a schematic illustration of the dry cutting process, PM sampling and particle size measurement arrangement (**d**)

m^3/h was collected on a quartz fiber filter using a $PM_{2.5}$ or PM_{10} impactor for chemical analysis or methylcellulose filter using a PM_{10} impactor for morphological analysis. The sampling process was started when the deepest point of the sawblade entered the sample material to get equal conditions over the whole sampling period. The sample collection was stopped before the foremost point of the sawblade left the sample material. PM was collected for 15 min for concrete and carbon grid samples and for 10 min for carbon rod samples. Three filters per sample material and PM size fraction were collected and stored at − 20 °C until analysis to gather information about the reproducibility of the dry cutting process. Chemical and morphological analysis were performed once for each filter.

2.3 Analytical Methods

2.3.1 On-Line Particle Size Determination

Particles produced during dry cutting of the materials were determined on-line with respect to the particle size and concentration using the aerosol particle sizer. In a sampling chamber, the particles are illuminated by a laser diode with 30 mW power and a wavelength of 660 nm. At the surface of the particles, the light is scattered dependent on the particle size. A photodetector at an angle of 90° to the particle beam measures the intensity of the scattered light. Based on the scattered light intensity and the number of signals, particle size distributions and concentrations per cm^3 and minute are recorded averaged over the whole sampling period. Particles can be measured with scattered light-equivalent diameters from 0.2 to 40 µm and concentrations of up to 10^4 particles/cm^3. Calibration was carried out in accordance with DIN ISO 21501 using 13 monodisperse particle size standards containing spherical polystyrene latex.

We acknowledge that an underestimation of particle diameters cannot be excluded. Since a mixture of rather spherical concrete and fibrous particles was measured, artifacts due to the measurement method could occur. The measured diameters are dependent on the shape of the particles, the absorption potential as well as the angle between light and particle in case of the fibers (Agimelen et al. 2017) and non-spherical concrete particles.

2.3.2 Scanning Electron Microscopy (SEM)

A scanning electron microscopy (SEM) device of the type "GeminiSEM 300" (Zeiss, Oberkochen, GER) was used to determine the occurrence and morphology of carbon fibers in the PM_{10} fractions. For the analysis, a circular segment of about 4 cm^2 was carefully cut out of the methylcellulose filter and fixed to a conducting tab ($d = 25$ mm), which was attached to an aluminum sample holder. The sample was sputtered with a 1–2 nm platinum layer to form a conducting surface, thus minimizing the induction of a charging process using a sputtering device of the type "SCD 040" (Bal-Tec, Pfäffikon, CHE). SEM measurements were done with an acceleration voltage of 2 keV and an operating distance of 4–5 mm. The magnifications 100×, 500×, 1000× and 5000× were used.

2.3.3 Thermo-Optical Carbon Analyzer–Photo Ionization Mass Spectrometry (TOCA-PIMS)

Filter punches with 8 mm in diameter were measured according to the Improve A protocol (Chow et al. 2007) with a thermo-optical carbon analyzer (TOCA) of the type "Model 2001 A" from Desert Research Institute (Reno, USA). This method yields information about the carbon composition of the PM fractions by thermally releasing carbon-containing substances from the PM, oxidizing them to carbon dioxide and subsequently reducing CO_2 to methane, which is quantified by a flame ionization detector (FID). The filter punches were heated stepwise under helium atmosphere to 140 °C, 280 °C, 480 °C and 580 °C to measure the organic carbon (OC) fractions OC1, OC2, OC3 and OC4, respectively. After reaching the baseline of the FID signal, the EC/OC switched to the next temperature. When all OC fractions were removed, the filter punch was further heated under helium/oxygen atmosphere (98%/2%) to 580 °C, 740 °C and 840 °C to measure the elemental carbon (EC) fractions EC1, EC2 and EC3, respectively. A laser beam irradiates the filter sample, and a decrease in laser transmission of the filter after OC2 indicates pyrolysis of the epoxy resin matrix during analysis. Therefore, the fractions OC1 and OC2 were combined to form the fraction thermal desorption OC. When oxygen was added, the laser transmission increases due to oxidation of the pyrolyzed material. Thus, the EC1 fraction was separated from an OC fraction OCpyro, which contains the pyrolyzed OC fraction, when the laser transmission crossed its baseline. Since OC3, OC4 and OCpyro most likely contain compounds from pyrolysis during the analysis, these fractions were combined to form the fraction pyrolysis OC.

For additional information about the organic fingerprint of the samples, the carbon analyzer was hyphenated to a photo ionization mass spectrometer (PIMS) (Grabowsky et al. 2011; Diab et al. 2015). Soft ionization was performed using resonance-enhanced multiphoton ionization (REMPI) using a wavelength of 248 nm produced by a krypton fluoride excimer laser of the type PhotonEx (Photonion GmbH, Schwerin, GER) with a repetition rate of 100 Hz and single photon ionization (SPI) using a wavelength of 118 nm produced by a Nd/YAG laser of the type "Spitlight 400" (InnoLas Photonics, Krailling, GER) with a repetition rate of 20 Hz equipped with a xenon gas cell to produce the third harmonic of the basic wavelength of 355 nm. In REMPI experiments, photons with an energy below the ionization energy of most compounds are used to excite the molecules to a metastable intermediate state. The energy of the intermediate state has to be in resonance to the REMPI wavelength. Afterwards, a second photon is used to ionize the molecule. In SPI experiments, the photon energy of 10.49 eV is higher than the ionization energies of most organic molecules (Boesl et al. 1994; Streibel and Zimmermann 2014; Zimmermann 2005; Boesl 2000; Butcher 1999). Hence, REMPI is a selective technique for aromatic compounds, while SPI can ionize almost all organic compounds. The TOCA-PIMS coupling is manufactured by Photonion GmbH (Schwerin, GER).

2.3.4 Comprehensive Two-Dimensional Gas Chromatography High-Resolution Time-of-Flight Mass Spectrometry (GC × GC-HRTOFMS)

Comprehensive two-dimensional gas chromatography high-resolution time-of-flight mass spectrometry (GC × GC-HRTOFMS) of the type "Pegasus HRT 4D" from Leco (St. Joseph, USA) equipped with a PTV injector "Atas Optic 4" from GL Sciences B.V. (Eindhoven, NL) was used to obtain structural information about organic compounds with the observed *m*/*z* values. Filter punches with 8 mm diameter were placed in the liner and organic compounds were injected via direct thermal desorption with a ramp rate of 50 K/s and a final temperature of 350 °C. Chromatographic separation was performed by a BPX50 column [60 m × 0.25 mm × 0.25 µm, SGE Analytical Science (Milton Keynes, UK)] in the first dimension and a BPX1 column [1 m × 0.1 mm × 0.1 µm, SGE Analytical Science (Milton Keynes, UK)] in the second dimension with an oven ramp of 3 K/min from 50 to 350 °C. Mass spectrometric analysis was performed in high-resolution mode with $R = 25{,}000$ and an electron ionization (EI) ion source.

2.3.5 Direct Thermal Desorption-Gas Chromatography/Mass Spectrometry (DTD-GC/MS)

Quantitative information about polycyclic aromatic hydrocarbons (PAH) and bisphenol A (BPA) was obtained by a direct thermal desorption gas chromatography mass spectrometer (DTD-GC/MS) of the type "GCMS-QP2010" from Shimadzu (Duisburg, GER) using deuterated internal standards. Thermal desorption was carried out within an "Atas Optic 4" from GL Sciences (Eindhoven, NL) with a ramp rate of 50 K/s and a final temperature of 350 °C. Chromatographic separation was performed by a BPX5 column [25 m × 0.22 mm × 0.25 µm, SGE Analytical Science (Milton Keynes, UK)] with a GC ramp of 20 K/min from 50 °C to 150 °C and then 5 K/min to 350 °C. Mass spectrometric analysis was done with an EI ion source. For quantitative analysis, data below a *S*/*N* ratio of 10 were not considered.

2.3.6 Carcinogenic Equivalent Assessment

The concentration of individual PAH was converted to ng/($m^3 \times cm^3$ cut material) to apply benzo(a)pyrene (BaP)-toxic equivalent factors (TEF) accordant to Nisbet and Lagoy (1992). By doing this, an assessment of the carcinogenic equivalents (BaP-TEQ) of investigated materials is possible. BaP-TEQ was calculated by multiplying the concentrations of each PAH compound with its TEF and the sum considered as carcinogenic equivalents. The corresponding concentrations in ng/($m^3 \times cm^3$ cut material) are summarized in the Supporting Information.

2.3.7 Statistical Evaluation

Differences in the number of particles, the carbon composition as well as PAH and BPA concentrations were evaluated using a student *t* test. Values below the quantification limit were set to be zero for calculations. Significance was set at $p < 0.05$. The corresponding *p* values are provided in the Supporting Information.

3 Results and Discussion

3.1 Physical Parameters

During the sample preparation, 2.22 mg/cm^3 cut material, 0.37 mg/cm^3, 4.07 mg/cm^3 and 2.96 mg/cm^3 of PM$_{2.5}$ and 2.78 mg/cm^3, 0.56 mg/cm^3, 7.41 mg/cm^3 and 6.56 mg/cm^3 of PM$_{10}$ were collected from the dry cutting simulation of carbon rods, carbon grids, C^3 and concrete, respectively. PM from the dry cutting simulation was at first evaluated according to their particle size distribution. Subsequently, the fibers were investigated with regards to the occurrence and morphology of contained carbon fibers.

3.1.1 Particle Size Distribution

Particle size distributions ($n = 6$) from the dry cutting simulation of the two reinforcement materials carbon rod and carbon grid as well as the C^3 and concrete reference material are shown in Fig. 2a.

More than 99% of the particles of all materials have a scattered light equivalent diameter < 10 µm. Dry cutting of the two reinforcement materials led to a high production of fine particles with a diameter of 0.2–0.5 µm of about 90% of the total particle counts. Differences between the rod-shaped and grid-shaped reinforcement materials could only be observed in the number of particles. Lower

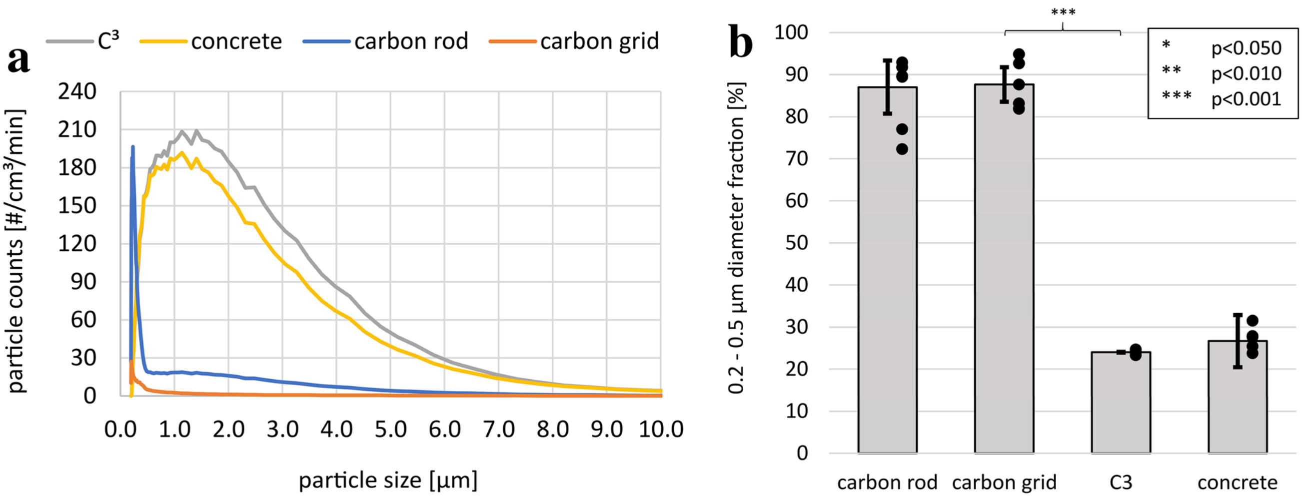

Fig. 2 Particle size distribution ($n = 6$, sizing limits: 0.2–40 µm, max. particle concentration: 10^4 particles/cm^3) of carbon rod*s*, carbon grid*s*, C^3 and concrete measured by a laser particle sizer during the dry cutting simulation. The reinforcement materials lead to a higher number of fine particles with a scattered light equivalent diameter of 0.2–0.5 µm **(a)**. A closer insight into the fraction with a diameter of 0.2–0.5 µm ($n = 6$) of the total particle counts of the different materials shows no significant differences between C^3 and concrete while high amounts of this fraction are observed in abrasive dust from the carbon grid **(b)**

particle concentrations were found for the grid-shaped reinforcement material for all particle sizes. Dry cutting of the C^3 and concrete samples led to larger particles with equal fractions of 0.2–0.5 µm, 0.5–1.0 µm and 1.0–2.5 µm in diameter of 25–30%. In total, a smaller fraction of particles with a diameter < 2.5 µm is formed during dry cutting of C^3 or concrete compared to the reinforcement materials with ~ 84% and 97%, respectively. Since a larger fraction of particles with a diameter of 0.2–0.5 µm is produced during dry cutting of the reinforcement materials, a more detailed view at this fraction is provided in Fig. 2b to investigate differences between the C^3 and the concrete particle size distribution. However, no significant difference could be observed.

3.1.2 Fiber Morphology/Occurrence

The PM$_{10}$ fractions were investigated toward fiber occurrence and their morphology using SEM. Figure 3 shows SEM pictures of fibers found in the PM$_{10}$ fractions of the C^3 material (a) and the carbon rods (b).

Only a few isolated fibers appeared in the abrasive PM from both reinforcement materials as well as the C^3. In accordance to the results of Bienkowski et al. (2018) and

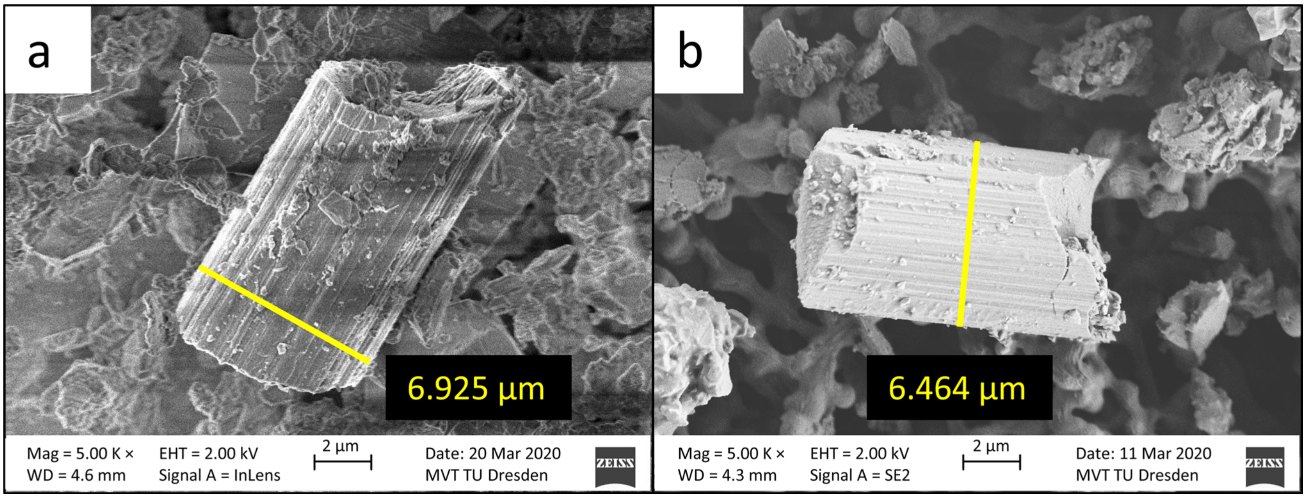

Fig. 3 Carbon fibers in the PM fraction PM$_{10}$ from a dry cutting simulation of a C^3 material **(a)** and a carbon rod **(b)**

Hillemann et al. (2018), all fibers have a diameter of ~ 7 µm which is the diameter of the fibers in the reinforcement materials due to the production process. On the surface of the fibers, the epoxy resin matrix material can be seen. While asbestos fibers tend to splice at the edges and form splint-like fiber fragments, sharp ruptures orthogonal to the fiber direction can be observed for the carbon fibers. Splint-like fibers and hence splicing of the fibers was not observed in the dry cutting simulation of the C^3 materials. Furthermore, harmful fibers according to the WHO (BAuA 2020) with a diameter < 3 µm, a length > 5 µm and a length-to-diameter ratio > 3 were not observed.

3.2 Chemical Parameters

In addition to physical parameters, the $PM_{2.5}$ and PM_{10} fractions were also investigated according to their chemical composition including their carbon composition and their organic fingerprint.

3.2.1 Carbon Composition

Given that the carbon fiber reinforcement materials consist of inorganic carbon fibers and an organic polymer matrix, the PM fractions $PM_{2.5}$ and PM_{10} are likely to contain both, elemental and organic carbon fractions. Figure 4 shows the carbon composition and total carbon content of the $PM_{2.5}$ and PM_{10} fractions of the two reinforcement materials as well as the C^3 material.

In $PM_{2.5}$, no difference between the two reinforcement materials can be observed. Both materials contain ~ 80% OC and only ~ 20% EC. The largest OC fraction is pyrolysis OC with ~ 60% of the total carbon content. While the carbon grid shows similar results in PM_{10}, the carbon rods contain only ~ 30% OC and ~ 70% EC. The largest OC fraction is also pyrolysis OC with ~ 25% of total carbon content. The different carbon composition refers to different mechanisms of PM formation for carbon rods in $PM_{2.5}$ and PM_{10} while no difference for the carbon grid was observed. While PM_{10} in a dry cutting process of carbon rods contains a larger number of particles that occur due to flake off of inorganic bulk material from the carbon fibers, $PM_{2.5}$ particles contain a high amount of the organic matrix material. Thus, the OC fraction in PM_{10} is smaller than in $PM_{2.5}$. $PM_{2.5}$ and PM_{10} from the carbon grid contain a high amount of the organic matrix material as well. Abrasive treatment of C^3 leads to a lower concentration of total carbon due to the vast amount of concrete PM. The carbon fraction consists of ~ 50% EC and ~ 50% OC in which the thermal desorption OC fraction is almost not present. Significant differences between $PM_{2.5}$ and PM_{10} of C^3 could not be observed.

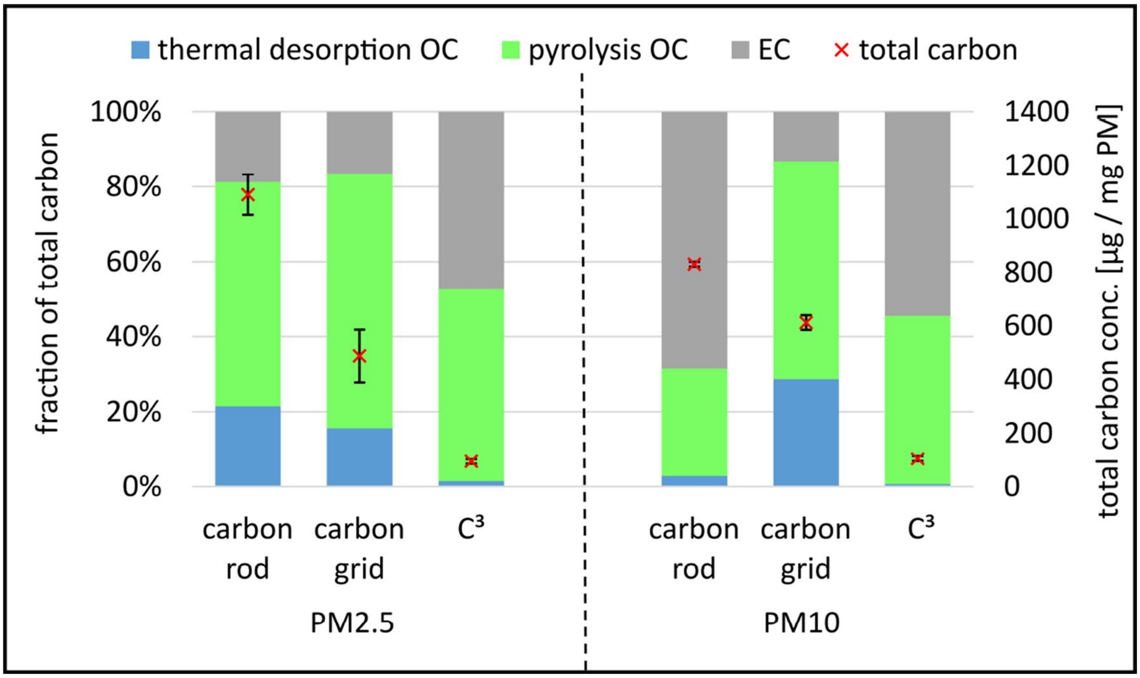

Fig. 4 Carbon composition and total carbon concentration ($n = 3$) in $PM_{2.5}$ and PM_{10} from a dry cutting simulation of C^3, carbon rods and carbon grids

3.2.2 Organic Fingerprint

The organic fractions were further investigated using time-of-flight mass spectrometry equipped with the soft ionization techniques REMPI and SPI. Figure 5 shows averaged REMPI (a) and SPI (b) spectra of the $PM_{2.5}$ thermal desorption OC fractions of the two reinforcement materials, the C^3 and the concrete reference.

Spectra of the $PM_{2.5}$ pyrolysis OC as well as the PM_{10} pyrolysis and thermal desorption OC fraction can be found in the Supplementary Information. It can be seen that the organic fingerprint of the two reinforcement materials carbon rod and carbon grid contain almost the same *m*/*z* pattern and thus, the same organic signature with only minor differences. REMPI experiments show several aromatic compounds with *m*/*z* values 228, 252 and 266 for both reinforcement materials and additionally *m*/*z* 304 for the carbon

Fig. 5 Organic fingerprint with labeled *m*/*z* values of the thermal desorption OC fraction of $PM_{2.5}$ from a dry cutting process of carbon rods, carbon grids, C^3 and concrete measured with a REMPI ion source as a selective soft ionization technique for aromatic compounds (n = 3, **a**) and SPI as a universal soft ionization technique for organic compounds with an ionization energy below 10.49 eV (n = 3, **b**)

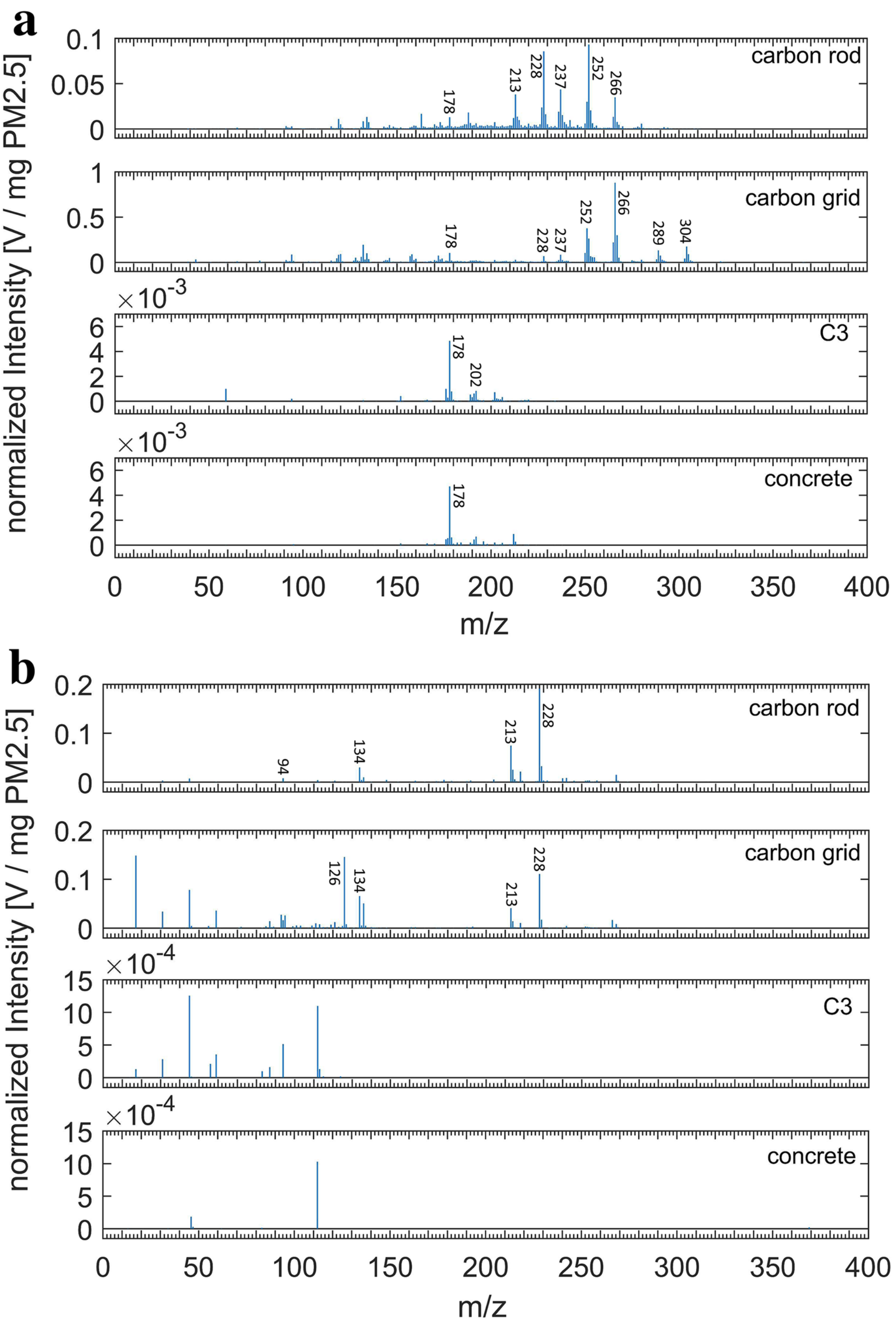

grid in the thermal desorption fraction. Furthermore, each of these compounds give a M-15 signal. Since REMPI is a comparatively soft ionization technique, only highly stabilized fragments can be observed. Hence, the M-15 signals can only be due to an easily removed methyl group and thus, the formation of a highly stabilized carbocation. In SPI experiments, compounds with the *m*/*z* values 228, 134 and 94 for both reinforcement materials and an additional signal at *m*/*z* 126 for the carbon grid can be observed. Similar to the REMPI experiments, *m*/*z* 228 gives a M-15 signal in the SPI experiment as well. In C^3 PM, none of these compounds can be observed. However, compounds with the *m*/*z* values 178 and 202 occur in PM from the reinforcement materials as well as the C^3 material. For concrete, *m*/*z* 178 could be observed as well. In the pyrolysis OC fractions, additional smaller *m*/*z* values between *m*/*z* 118 and *m*/*z* 192 due to pyrolysis of organic compounds during the analysis can be found. In contrast to the thermal desorption fraction, the same signals as for the carbon grid can be found for the C^3 material but not for concrete in the pyrolysis fraction. $PM_{2.5}$ and PM_{10} only differ in their signal intensities.

3.2.3 Evaluation of Compounds

To obtain more structural information about the unknown compounds, filters were additionally analyzed by GC × GC-HRTOFMS. Thermal desorption of filters was used for sample introduction, which ensures good comparability to the combined fractions OC1 and OC2 from the TOCA-PIMS. Detected compounds, which contained *m*/*z* 94, *m*/*z* 126, *m*/*z* 134 and *m*/*z* 228 in their mass spectra, could be identified as phenol, melamine, 4-isopropenylphenol and bisphenol A by spectral comparison with the NIST database. BPA is the main component of most commercially available epoxy resins. Furthermore, phenol and 4-isopropenylphenol are known pyrolysis products of epoxy resins based on BPA (Wang et al. 2016; Nakagawa and Tsuge 1987; Yamada et al. 1995; Luda et al. 2010). Since melamine is a polyvalent amine, it is used as a curing agent for epoxy resins.

Compounds which could not be identified by spectral comparison with the NIST database were evaluated by manual interpretation of the mass spectra and retention time region. Figure 6a shows exemplarily the GC × GC chromatogram of the $PM_{2.5}$ fraction from dry cutting of the carbon grid. It can be observed that the unknown compounds with *m*/*z* 252, *m*/*z* 266 and *m*/*z* 304 as well as the identified BPA (*m*/*z* 228) only vary in the first chromatographic dimension which means that they are most likely all of the compound class of BPA. Figure 6b–e shows the GC × GC-HRTOFMS mass spectra of BPA and the unknown compounds as well as their proposed structures.

By means of the exact masses, the sum formulas of *m*/*z* 252, *m*/*z* 266 and *m*/*z* 304 could be assigned to $C_{17}H_{16}O_2$, $C_{18}H_{18}O_2$ and $C_{21}H_{20}O_2$, respectively. Peaks with the exact masses of 91.0543 and 119.0491 can be observed for the compounds with *m*/*z* 252 and 266 as well as BPA. Hence, these compounds are similar to BPA on one side of the molecule, which leads to the formation of the same EI fragments. Furthermore, all of these compounds show a M-15 signal. Since the sum formula $C_{17}H_{16}O_2$ of the compound with *m*/*z* 252 contains two additional carbon atoms compared to BPA, only two derivatives of BPA would be possible, a terminal alkyne or a benzofuran. Due to the fact that terminal alkynes are comparatively instable, a benzofuran is more likely. Moreover, Wang et al. (2016) identified this compound as a pyrolysis product of epoxy resins. The sum formula of the compound with *m*/*z* 266 differs from *m*/*z* 252 by an additional methyl group.

The compound with *m*/*z* 304 shows the same *m*/*z* pattern, but the peaks 128.0621 and 157.0649 are shifted to higher *m*/*z* ratios by half of the mass difference to BPA. Hence, both sides of the molecule are substituted by the same chemical group which is similar to the substituent of the compound with *m*/*z* 266. Thus, we propose the chemical structure shown in Fig. 6e. Due to a + M effect of the two aromatic systems, all of these molecules could easily form stable M-15 carbocations by abstraction of a central methyl group. A detailed list of organic compounds found in the PM is given in Table 1.

Many of these compounds were also found in pyrolysis studies on epoxy resins based on BPA (Wang et al. 2016, 2010; Nakagawa and Tsuge 1987; Yamada et al. 1995; Luda et al. 2010; Zhang et al. 2018; Balabanovich et al. 2005). Thus, at the edge of the sawblade, pyrolysis of the epoxy resin matrix contained in the reinforcement materials takes place.

3.2.4 BPA and PAHs Quantification

BPA is well known as an endocrine disruptor. High concentrations might be harmful to human health by impairing the reproduction system or liver and kidney function (Rochester 2013). Polycyclic aromatic hydrocarbons are known to be carcinogenic (Armstrong et al. 2004). Thus, it is important to evaluate how much BPA and PAHs are released during dry cutting processes of C^3 materials to protect the operating employees. Figure 7 shows the measured concentrations of BPA (a) and the PAH pyrene (b). In addition to pyrene, phenanthrene, anthracene and fluoranthene were also detected. The concentrations of all PAHs and BPA are summarized in Table 2.

BPA is found in the PM of the reinforcement materials in comparatively high concentrations of up to 383 µg/mg. No significant difference could be found between $PM_{2.5}$ and PM_{10}. PM from the carbon grid and carbon rod also show comparable values. Since BPA is a monomer of the epoxy

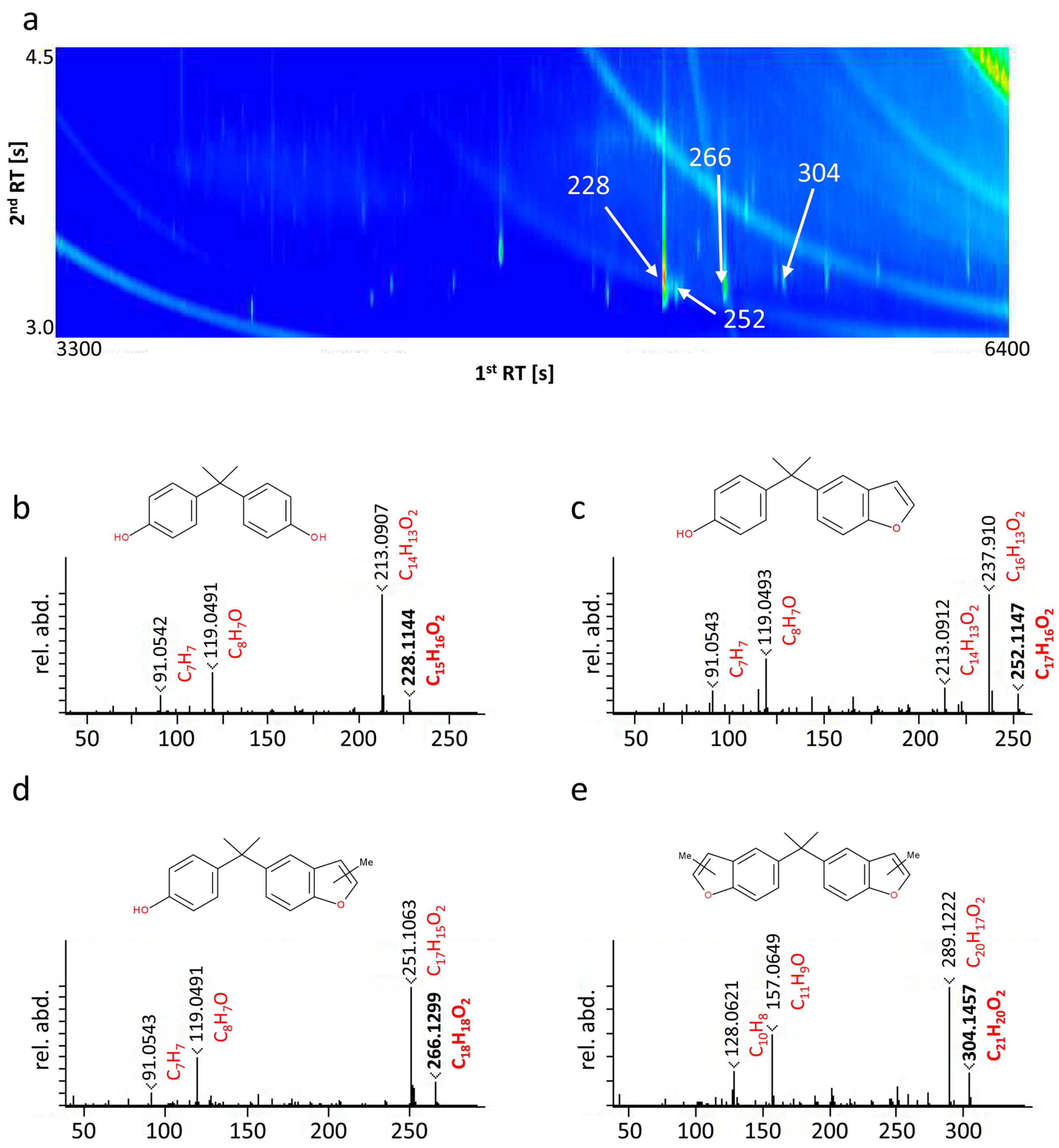

Fig. 6 Representation of the 2D-Contour plot of the GC×GC-HRTOFMS measurement of $PM_{2.5}$ from dry cutting simulation of carbon grid (**a**). Peaks which contain the molecular ions *m*/*z* 228, 252, 266 and 304 are highlighted. EI mass spectra of the four highlighted peaks are shown for *m*/*z* 228 (**b**), 252 (**c**), 266 (**d**) and 304 (**e**). Assigned elemental composition for exact masses of the most abundant ions are depicted in red. Shown structures represent the suggestions for the unknown compounds based on the EI-fragmentation pattern

resin matrix of the reinforcement materials, this concentration is most likely due to BPA as a pyrolysis product of the epoxy resin at the sawblade edge during the dry cutting simulation. However, in the C^3 PM, the BPA concentration is much lower with up to 32.9 µg/mg due to a dilution with concrete PM. Furthermore, the BPA concentration in $PM_{2.5}$ of the C^3 is slightly higher than that in the PM_{10} fraction with 24.9 µg/mg.

Table 1 Organic compounds in the inhalable PM fractions $PM_{2.5}$ and PM_{10} of carbon rods and carbon grids from a dry cutting simulation

m/z	compound	carbon rod	carbon grid
304	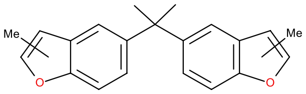		X
266	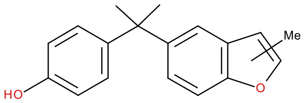	X	X
252	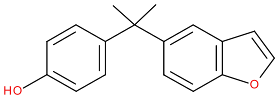	X	X
228	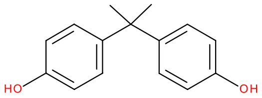	X	X
202	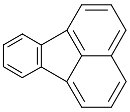 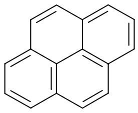	X	X
178	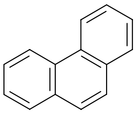 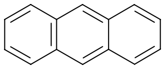	X	X
134	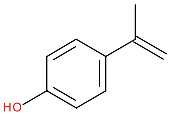	X	X
126	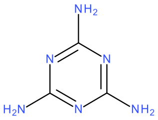		X
94	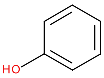	X	X

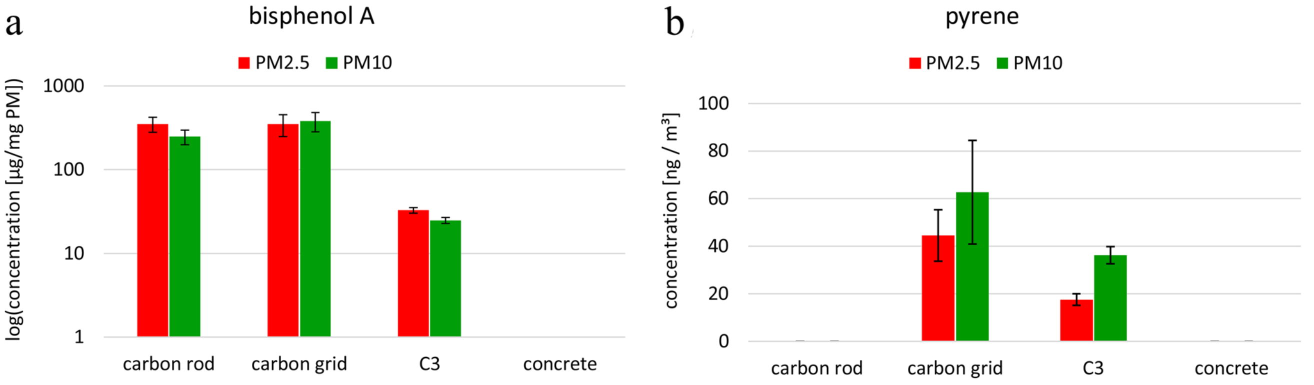

Fig. 7 Concentrations of BPA (**a**) and pyrene (**b**) in the inhalable PM fractions $PM_{2.5}$ and PM_{10} from a dry cutting simulation of C^3 reinforcement materials, C^3 and concrete measured by DTD-GC/MS using deuterated internal standards ($n = 3$)

Table 2 Concentrations of BPA and the PAHs phenanthrene, anthracene, fluoranthene and pyrene in the inhalable PM fractions $PM_{2.5}$ and PM_{10} from a dry cutting simulation of carbon rods, carbon grids, C^3 and concrete measured by DTD-GC/MS using deuterated internal standards (*n* = 3)

	Carbon rod		Carbon grid		C^3		Concrete	
	$PM_{2.5}$	PM_{10}	$PM_{2.5}$	PM_{10}	$PM_{2.5}$	PM_{10}	$PM_{2.5}$	PM_{10}
Bisphenol A [µg/mg PM]	350.8 ± 50.6	247.5 ± 33.9	352.3 ± 73.4	382.6 ± 68.9	32.9 ± 1.9	24.9 ± 1.5	n.d	n.d
Phenanthrene [ng/mg PM]	3.19 ± 0.55	1.34 ± 0.28	28.18 ± 5.93	41.78 ± 7.39	2.71 ± 0.07	2.04 ± 0.21	n.d	n.d
Anthracene [ng/mg PM]	n.d	n.d	4.74 ± 0.70	6.77 ± 1.27	0.43 ± 0.01	0.28 ± 0.02	n.d	n.d
Fluoranthene [ng/mg PM]	0.34 ± 0.15	1.19 ± 0.18	15.59 ± 3.00	18.79 ± 2.22	0.40 ± 0.02	0.52 ± 0.08	n.d	n.d
Pyrene [ng/mg PM]	n.d	n.d	12.01 ± 2.52	12.78 ± 1.70	0.32 ± 0.02	0.40 ± 0.06	n.d	n.d

n.d. not detected

In animal studies, doses in the low µg/kg body weight (BW) range already showed significant effects on the reproduction system and allergic asthmatic responses (Meng et al. 2018; Yanagisawa et al. 2019). Exposure rates per cm^3 cut material can be calculated according to the formula

$$\mathrm{ER} = \frac{\text{BPA conc.} \times \text{IR}}{\text{BW}} \tag{1}$$

with ER = exposure rate in µg/(min × kg BW × cm^3 cut material), BW = body weight in kg, BPA conc. = concentration of BPA in µg/(m^3 × cm^3 cut material) and IR = inhalation rate in m^3/min. Considering the inhalation rate, a 30-year-old standard person (male, 70 kg) at a high intensity inhalation [8.21×10^{-2} m^3/min (95th percentile, US EPA 2011)] would be exposed to 5.1 µg BPA/kg BW × min × cm^3 cut material, 0.6 µg BPA/kg BW × min × cm^3 cut material and 0.8 µg BPA/kg BW × min × cm^3 cut material from $PM_{2.5}$ of carbon rods, carbon grids and C^3, respectively. Hence, it is highly recommended to use polymer matrices in the C^3 reinforcement production which are not based on BPA monomers. Furthermore, we recommend to wear particle masks and to minimize the PM during abrasive treatment of C^3 using suction devices and wet cutting processes.

The PAH concentrations are found to be four orders of magnitude lower compared to BPA. Phenanthrene gave the highest PAH concentrations with up to 41.8 ng/mg in the carbon grid dust. Carbon rods gave much lower concentrations of up to 3.2 ng/mg. The concentrations of anthracene, fluoranthene and pyrene in PM of the carbon grid are up to 6.8 ng/mg, 18.8 ng/mg and 12.8 ng/mg, respectively. In PM of the carbon rod, only fluoranthene with concentrations of up to 1.2 ng/mg was present in addition to phenanthrene. PAHs occur during pyrolysis of most organic polymers. In PM from the C^3, the PAH concentrations were much lower than for the carbon grid with up to 2.7 ng/mg, 0.4 ng/mg, 0.5 ng/mg and 0.4 ng/mg for phenanthrene, anthracene, fluoranthene and pyrene, respectively. The lower concentrations are due to dilution with concrete PM and fewer carbon grid layers in the C^3 that were cut through. Differences between the $PM_{2.5}$ and the PM_{10} fractions could not be observed. The PM from the concrete reference sample contained no measurable concentrations of PAHs or BPA.

3.2.5 Carcinogenic Risk Associated to PM Fractions

The contribution of each PAH in the different PM fractions of tested materials to the carcinogenic potency relative to BaP normalized to the cut volume in cm^3 is shown in Table 3. The grid-shaped reinforcement material showed the higher BaP-TEQ values, which were elevated in the PM_{10}

Table 3 BaP-equivalent carcinogenicity risk assessed in PM fractions of investigated materials (ng/m^3) normalized to the cut volume in cm^3

	TEF	BaP-TEQ levels							
		Carbon rod		Carbon grid		C^3		Concrete	
		$PM_{2.5}$	PM_{10}	$PM_{2.5}$	PM_{10}	$PM_{2.5}$	PM_{10}	$PM_{2.5}$	PM_{10}
Phenanthrene [ng/m^3 PM]	0.001	0.042	0.024	0.039	0.076	0.055	0.072	n.d	n.d
Anthracene [ng/m^3 PM]	0.01	n.d	n.d	0.066	0.124	0.087	0.096	n.d	n.d
Fluoranthene [ng/m^3 PM]	0.001	0.004	0.019	0.022	0.034	0.008	0.018	n.d	n.d
Pyrene [ng/m^3 PM]	0.001	n.d	n.d	0.016	0.023	0.006	0.013	n.d	n.d
Σ_4 PAHs		0.05 ± 0.01	0.04 ± 0.01	0.14 ± 0.02	0.26 ± 0.06	0.16 ± 0.01	0.20 ± 0.03	n.d	n.d

n.d. not detected

fraction compared to the $PM_{2.5}$ due to the considerable contribution of anthracene. The carcinogenicity potency of carbon grid was up to 7 times higher with respect to carbon rod-shaped reinforcement material. A significant effect of the grid-shaped reinforcement material was found in both $PM_{2.5}$ and PM_{10} formed during the dry cutting of C^3 with a slight difference between the two PM fractions.

We acknowledge that the potential risk of PAH exposure based on BaP-TEQ may be misjudged due to possible PAH synergistic interactions or their chemical degradation by aerosol oxidant levels and photochemical reactions that can generate nitrated/oxygenated PAHs known to be more toxic than their derivative PAHs.

4 Conclusions

In this study, the inhalable PM fractions $PM_{2.5}$ and PM_{10} formed during dry cutting of C^3 and their reinforcement materials were investigated toward the occurrence of toxic components. Since C^3 reinforcement materials contain inorganic carbon fibers as well as an organic matrix, toxicity can be due to harmful fibers or organic compounds.

Analysis of the carbon composition showed that the ratio between elemental carbon and organic carbon in PM_{10} is dependent on the shape of the reinforcement material due to different mechanisms of PM formation. This could have an impact on the toxicity of the abrasive dust from different reinforcement materials.

According to the WHO, fibers with a length > 5 µm, a diameter < 3 µm and a length-to-diameter ratio > 3 are considered to have harmful effects on human health (BAuA 2020). In PM from dry cutting of C^3 and its reinforcement materials, no harmful fibers according to this definition were observed. Furthermore, no splint-like fibers can be found, which indicates that no splicing of the fibers occurs like it is seen in asbestos concrete. This suggests, that the risk of fiber toxicity from cutting of C^3 pieces can be rated low.

However, domestic fires and thermal recycling of C^3 could lead to a reduction in fiber diameter and thus, the formation of harmful fibers (Cerny et al. 2007; Eibl 2017). Therefore, future experiments should address, what happens in cutting or other machining processes of C^3 materials, which were exposed to increased temperatures.

In contrast, the organic compounds BPA as well as the PAHs phenanthrene, anthracene, fluoranthene and pyrene occurred in the $PM_{2.5}$ and PM_{10} fractions of C^3 and its reinforcement materials due to pyrolysis of the organic matrix at the edge of the sawblade. Derivatives of BPA were additionally found in abrasive dust from the reinforcement materials. Quantitative analysis showed that comparatively high concentrations of BPA are contained in the inhalable PM from dry cutting processes of C^3 and its reinforcement materials. We acknowledge, that an overestimation of the BPA concentrations cannot be excluded due to the formation of artifacts during the applied thermal desorption-based methods. BPA is a well-known endocrine disruptor that can impair the reproduction system as well as the liver and kidney function (Rochester 2013). PAHs are carcinogenic (Armstrong et al. 2004) and the potential carcinogenic risk evaluated in this study clearly showed different harmful contributions of reinforcement materials to the concrete generated abrasive dust. Hence, we recommend to use organic matrix materials that are not based on BPA and to take the pyrolysis products of the considered organic matrix material into account during the manufacturing process of C^3 reinforcement materials. We further recommend that workers should wear particle protection masks and that the PM emission should be minimized using wet cutting processes and a suction device during C^3 treatment.

However, no direct information about the toxicity of dust from C^3 material machining is given in this work. Studies to address the question, whether increased toxicity of PM from C^3 machining can be observed in in vitro experiments with human lung cells are currently underway.

Supplementary Information The online version contains supplementary material available at https://doi.org/10.1007/s41810-021-00103-8.

Acknowledgements The authors thank the colleagues from the Institute of Construction Management at the TU Dresden for providing the C^3 samples.

Author Contributions All authors have contributed to the work of this paper. All authors read and approved the final manuscript.

Funding Open Access funding enabled and organized by Projekt DEAL. This research is part of the C^3-Carbon Concrete Composites project funded by the German Federal Ministry of Education and Research in the loan program "Zwanzig20-Partnerschaft für Innovation".

Availability of Data and Materials The experimental data used to support the observations of this study are included in the article and its supporting information.

Declarations

Conflict of interest On behalf of all authors, the corresponding author states that there is no conflict of interest.

References

Agimelen OS, Mulholland AJ, Sefcik J (2017) Modelling of artefacts in estimations of particle size of needle-like particles from laser diffraction measurements. Chem Eng Sci 158:445–452. https://doi.org/10.1016/j.ces.2016.10.031

Armstrong B, Hutchinson E, Unwin J, Fletcher T (2004) Lung cancer risk after exposure to polycyclic aromatic hydrocarbons: a review and meta-analysis. Environ Health Perspect 112(9):970–978. https://doi.org/10.1289/ehp.6895

Balabanovich AI, Luda MP, Operti L (2005) GC/MS identification of pyrolysis products from fire-retardant brominated epoxy resin. J Fire Sci 23:227–245. https://doi.org/10.1177/0734904105047006

BAuA (2020) TRGS 905: verzeichnis krebserzeugender, keimzellmutagener oder reproduktionstoxischer Stoffe. In: Technische Regeln für Gefahrstoffe. https://www.baua.de/DE/Angebote/Rechtstexte-und-Technische-Regeln/Regelwerk/TRGS/pdf/TRGS-905.pdf?__blob=publicationFile. Accessed 08 Jan 2021

Bienkowski N, Hillemann L, Streibel T, Kortmann J, Kopf F, Zimmermann R, Jehle P (2018) Bearbeitung von Carbonbeton—eine bauverfahrenstechnische und medizinische Betrachtung. In: VDI-Bautechnik—Jahresausgabe 2017/2018, pp 110–117

Boesl U (2000) Laser mass spectrometry for environmental and industrial chemical trace analysis. J Mass Spectrom 35:289–304. https://doi.org/10.1002/(SICI)1096-9888(200003)35:3%3c289::AID-JMS960%3e3.0.CO;2-Y

Boesl U, Zimmermann R, Weickhardt C, Lenoir D, Schramm K-W, Kettrup A, Schlag EW (1994) Resonance-enhanced multi-photon ionization: a species-selective ion source for analytical time-of flight mass spectrometry. Chemosphere 29(7):1429–1440. https://doi.org/10.1016/0045-6535(94)90276-3

Böhm R, Thieme M, Wohlfahrt D, Wolz DS, Richter B, Jäger H (2018) Reinforcement systems for carbon concrete composites based on low-cost carbon fibers. Fibers 6:56. https://doi.org/10.3390/fib6030056

Butcher DJ (1999) Vacuum ultraviolet radiation for single-photoionization mass spectrometry: a review. Microchem J 62:354–362. https://doi.org/10.1006/mchj.1999.1745

Cerny R, Nemeckova J, Rovnanikova P, Bayer P (2007) Effect of thermal decomposition processes on the thermal properties of carbon fiber reinforced cement composites in high-temperature range. J Therm Anal Calorim 90(2):475–488. https://doi.org/10.1007/s10973-006-7944-0

Chow JC, Watson JG, Chen L-WA, Chang MCO, Robinson NF, Trimble D, Kohl S (2007) The IMPROVE_A temperature protocol for thermal/optical carbon analysis: maintaining consistency with a long-term database. J Air Waste Manage 57:1014–1023. https://doi.org/10.3155/1047-3289.57.9.1014

Chung DDL (2000) Cement reinforced with short carbon fibers: a multifunctional material. Compos B Eng 31:511–526. https://doi.org/10.1016/S1359-8368(99)00071-2

Diab J, Streibel T, Cavalli F, Lee SC, Saathoff H, Mamakos A, Chow JC, Chen L-WA, Watson JG, Sippula O, Zimmermann R (2015) Hyphenation of a EC/OC thermal-optical carbon analyzer to photo-ionization time-of-flight mass spectrometry: an off-line aerosol mass spectrometric approach for characterization of primary and secondary particulate matter. Atmos Meas Tech 8:3337–3353. https://doi.org/10.5194/amt-8-3337-2015

Eibl S (2017) Potential for the formation of respirable fibers in carbon fiber reinforced plastic materials after combustion. Fire Mater 41:808–816. https://doi.org/10.1002/fam.2423

Felley-Bosco E, MacFarlane M (2018) Asbestos: modern insights for toxicology in the era of engineered nanomaterials. Chem Res Toxicol 31:994–1008. https://doi.org/10.1021/acs.chemrestox.8b00146

Fiore V, Scalici T, Di Bella G, Valenza A (2015) A review on basalt fibre and its composites. Compos B Eng 74:74–94. https://doi.org/10.1016/j.compositesb.2014.12.034

Frank E, Steudle LM, Ingildeev D, Spörl JM, Buchmeiser MR (2014) Carbon fibers: precursor systems, processing, structure, and properties. Angew Chem Int 53:5262–5298. https://doi.org/10.1002/anie.201306129

Ghugal YM, Deshmukh SB (2006) Performance of alkali-resistant glass fiber reinforced concrete. J Reinf Plast Comp 25(6):617–630. https://doi.org/10.1177/0731684405058273

Grabowsky J, Streibel T, Sklorz M, Chow JC, Watson JG, Mamakos A, Zimmermann R (2011) Hyphenation of a carbon analyzer to photo-ionization mass spectrometry to unravel the organic composition of particulate matter on molecular level. Anal Bioanal Chem 401:3153–3164. https://doi.org/10.1007/s00216-011-5425-1

Harrison RM, Yin J (2000) Particulate matter in the atmosphere: which particle properties are important for its effects on health. Sci Total Environ 249:85–101. https://doi.org/10.1016/s0048-9697(99)00513-6

Hillemann L, Stintz M, Streibel T, Zimmermann R, Öder S, Kasurinen S, Di Bucchianico S, Kanashova T, Dittmar G, Konzack D, Große S, Rudolph A, Berger M, Krebs T, Saraji-Bozorgzad MR, Walte A (2018) Charakterisierung von Partikelemissionen aus dem Trennschleifprozess von kohlefaserverstärktem Beton (Carbonbeton). Gefahrstoffe Reinhalt Luft 78(6):230–240

Jäger H, Cherif C, Kirsten M, Behnisch T, Wolz DS, Böhm R, Gude M (2016) Influence of processing parameters on the properties of carbon fibres—an overview. Mat-Wiss u Werkstofftech 47(11):1044–1057. https://doi.org/10.1002/mawe.201600630

Kim K-H, Kabir E, Kabir S (2015) A review on the human health impact of airborne particulate matter. Environ Int 74:136–143. https://doi.org/10.1016/j.envint.2014.10.005

Kizilkanat AB, Kabay N, Akyüncü V, Chowdhury S, Akça AH (2015) Mechanical properties and fracture behavior of basalt and glass fiber reinforced concrete: an experimental study. Constr Build Mater 100:218–224. https://doi.org/10.1016/j.conbuildmat.2015.10.006

Lee JJ, Song J, Kim H (2014) Chemical stability of basalt fiber in alkaline solution. Fibers Polym 15(11):2329–2334. https://doi.org/10.1007/s12221-014-2329-7

Lenain JC, Bunsell AR (1979) The resistance to crack growth of asbestos cement. J Mater Sci 14:321–332. https://doi.org/10.1007/BF00589822

Luda MP, Balabanovich AI, Zanetti M (2010) Pyrolysis of fire retardant anhydride-cured epoxy resins. J Anal Appl Pyrol 88:39–52. https://doi.org/10.1016/j.jaap.2010.02.008

Mai YW (1979) Strength and fracture properties of asbestos-cement mortar composites. J Mater Sci 14:2091–2102. https://doi.org/10.1007/BF00688413

Meng Y, Lin R, Wu F, Sun Q, Jia L (2018) Decreased capacity for sperm production induced by perinatal bisphenol a exposure is associated with an increased inflammatory response in the offspring of C57BL/6 male mice. Int J Environ Res Public Health 15:2158. https://doi.org/10.3390/ijerph15102158

Morgan P (2005) Carbon fibers and their composites, 1st edn. Taylor & Francis Group, Boca Raton, pp 121–322

Nakagawa H, Tsuge S (1987) Studies on thermal degradation of epoxy resins by high-resolution pyrolysis gas-chromatography. J Anal

Appl Pyrol 12:97–113. https://doi.org/10.1016/0165-2370(87)85060-X

Nisbet IC, LaGoy PK (1992) Toxic equivalency factors (TEFs) for polycyclic aromatic hydrocarbons (PAHs). Regul Toxicol Pharmacol 16(3):290–300. https://doi.org/10.1016/0273-2300(92)90009-x

Rochester JR (2013) Bisphenol A and human health: a review of the literature. Reprod Toxicol 42:132–155. https://doi.org/10.1016/j.reprotox.2013.08.008

Sim J, Park C, Moon DY (2005) Characteristics of basalt fiber as a strengthening material for concrete structures. Compos B Eng 36:504–512. https://doi.org/10.1016/j.compositesb.2005.02.002

Spelter A, Bergmann S, Bielak J, Hegger J (2019) Long-term durability of carbon-reinforced concrete: an overview and experimental investigations. Appl Sci 9:1651. https://doi.org/10.3390/app9081651

Streibel T, Zimmermann R (2014) Resonance-enhanced multiphoton ionization mass spectrometry (REMPI-MS): applications for process analysis. Annu Rev Anal Chem 7:361–381. https://doi.org/10.1146/annurev-anchem-062012-092648

US EPA (2011) Exposure Factors Handbook 2011 Edition (Final Report). U.S. Environmental Protection Agency, Washington, DC; EPA/600/R-09/052F, pp 6–42

Wang C, Li K, Li H, Jiao G, Lu J, Hou D (2008) Effect of carbon fiber dispersion on the mechanical properties of carbon fiber-reinforced cement-based composites. Mater Sci Eng A 487:52–57. https://doi.org/10.1016/j.msea.2007.09.073

Wang X, Hu Y, Song L, Xing W, Lu H (2010) Thermal degradation behaviors of epoxy resin/POSS hybrids and phosphorus-silicon synergism of flame retardancy. J Polym Sci B Polym Phys 48:693–705. https://doi.org/10.1002/polb.21939

Wang P, Yang F, Li L, Cai Z (2016) Flame retardancy and mechanical properties of epoxy thermosets modified with a novel DOPO-based oligomer. Polym Degrad Stabil 129:156–167. https://doi.org/10.1016/j.polymdegradstab.2016.04.005

Weiler L, Vollpracht A (2019) Environmental compatibility of carbon reinforced concrete: irrigated construction elements. Key Eng Mater 809:314–319. https://doi.org/10.4028/www.scientific.net/KEM.809.314

Yamada T, Okumoto T, Ohtani H, Tsuge S (1995) Characterization of epoxy resins cured with dicyandiamide in the presence of imidazole catalysts by high-resolution pyrolysis-gas chromatography. J Anal Appl Pyrol 33:157–166. https://doi.org/10.1016/0165-2370(94)00876-3

Yanagisawa R, Koike E, Win-Shwe T-T, Takano H (2019) Oral exposure to low dose bisphenol A aggravates allergic airway inflammation in mice. Toxicol Rep 6:1253–1262. https://doi.org/10.1016/j.toxrep.2019.11.012

Zhang W, Fina A, Ferraro G, Yang R (2018) FTIR and GCMS analysis of epoxy resin decomposition products feeding the flame during UL94 standard flammability test. Application to the understanding of the blowing-out effect in epoxy/polyhedral silsesquioxane formulations. J Anal Appl Pyrol 135:271–280. https://doi.org/10.1016/j.jaap.2018.08.026

Zimmermann R (2005) Laser ionisation mass spectrometry for online analysis of complex gas mixtures and combustion effluents. Anal Bioanal Chem 381:57–60. https://doi.org/10.1007/s00216-004-2886-5